All-optical coherent control of electrical currents in centrosymmetric semiconductors

Marko Spasenović, Markus Betz, Louis Costa, and Henry M. van Driel
Department of Physics and Institute for Optical Sciences, University of Toronto, Toronto, Ontario, Canada M5S 1A7
(Received 26 September 2007; revised manuscript received 30 November 2007; published 4 February 2008)

The absorption of phase-related near-infrared fundamental (ω, 0.7 eV $\leqslant \hbar\omega \leqslant$ 0.9 eV) and second harmonic (2ω) pulses of 150 fs duration results in ballistic electrical currents in clean bulk germanium and silicon at room temperature. The ultrafast charge motion is directly monitored via a time-resolved analysis of the emitted bursts of terahertz radiation. The current generation process relies on a third-order optical nonlinearity with a current injection efficiency only slightly reduced compared to the established current injection in direct-gap semiconductors such as GaAs. In the present case, current injection takes place across the direct band gap of germanium, whereas it involves indirect optical transitions in silicon. The vector direction of the current is defined by the polarization of the two-color pump field and the relative phase $\Delta\Phi = 2\Phi_{\omega} - \Phi_{2\omega}$. Microscopically, current injection can be understood as arising from the quantum interference of one- and two-photon absorption processes. In the case of silicon, these indirect optical transitions may involve different types of phonons and can occur via numerous pathways. We therefore propose a model based on third-order perturbation theory which qualitatively explains why a current injection can occur across an indirect band gap.

DOI: 10.1103/PhysRevB.77.085201 PACS number(s): 78.47.−p

I. INTRODUCTION

Charge transport in elementary group IV semiconductors such as silicon and germanium as well as their alloys are a central area of modern semiconductor physics. In particular, silicon based integrated devices are the cornerstone of both electronics and information technology. The strong relevance of group IV semiconductors in electronics is in strong contrast to their minor role in photonics. This is mainly due to the weak interaction with light related to the indirect band gap of these materials. The diamond lattice also has inversion symmetry and, therefore, these materials do not possess a second-order optical nonlinearity. Recently, interest in silicon photonics has increased substantially as techniques have been found to circumvent these limitations.[1] Specifically, clever strategies such as nanostructuring, quantum confinement, or strain have been employed to implement optical functionalities within the established silicon platform.[2–5]

Control over the motion of charge carriers in semiconductors is traditionally achieved by purely electronic means. However, in direct band-gap materials such as GaAs, efficient ways to all-optically generate directional currents have been realized. For example, illuminating GaAs with harmonically related near-infrared femtosecond pulses results in the injection of a ballistic current.[6] This third-order nonlinear optical process relies on the interference of one- and two-photon absorption pathways involving valence and conduction band states near the Γ point of the Brillouin zone. However, this unique all-optical control of the vector direction of ultrafast electrical currents might be considered unlikely especially in an indirect band gap material such as silicon with its complex conduction band structure and phonon-assisted absorption.

In this paper, we report the generation of coherently controlled photocurrents in unbiased bulk silicon and germanium specimens using near-infrared pulses synthesized from a femtosecond fundamental beam (ω) and its second harmonic (2ω). We, hereby, enlarge on the recent short report on all-optical current injection in silicon.[7] The charge dynamics in the semiconductor layer is directly monitored via a time-resolved analysis of the emitted terahertz radiation. We show that these photocurrents can be controlled by the phase, polarization, and intensity of the excitation beams. Although both germanium and silicon are indirect semiconductors, the wavelengths of this study (fundamental wavelengths 1420 nm $\leqslant \lambda \leqslant$ 1800 nm) couple direct optical transitions in germanium but indirect transitions in silicon. However, the current injection strength in silicon is comparable to germanium, i.e., the efficiency of the current injection after correcting for the different absorption properties is not strongly affected by the excitation across the indirect band gap. The present paper is organized as follows: some general aspects of coherence driven electrical currents in semiconductors are summarized in Sec. II. The experimental scheme for the generation of phase-stable superpositions of near-infrared pulses and the electro-optic detection of the emitted terahertz radiation is presented in Sec. III. Section IV is related to current injection in germanium where current injection occurs across the direct band gap, i.e., similar to the case of direct band-gap materials such as GaAs. Special attention is paid to the investigation of the polarization geometry of the experiment. In Sec. V, the concept of current injection is transferred to bulk silicon. In this case, the current injection purely relies on the indirect, phonon-assisted excitation across the indirect band gap. The influence of the excitation wavelength is studied in detail. Section VI serves to provide qualitative theoretical insight into the current injection across the indirect band gap based on an analysis of the dominant transition rates for phonon-assisted one- and two-photon absorptions.

II. GENERAL CONSIDERATION ABOUT ALL-OPTICAL CURRENT INJECTION IN SEMICONDUCTORS

The discussion of optically induced currents in direct-gap materials such as GaAs and InP, where theoretically and experimentally much more is known, serves as a useful starting

 ©2008 The American Physical Society

point for the discussion of the current injection mechanism in centrosymmetric media. Zinc blende materials are noncentrosymmetric and, consequently, have a nonzero second-order optical nonlinearity. Second-order current injection is governed by $\chi^{(2)}(0;\omega,-\omega)$ and occurs via optical rectification,[8,9] the excitation of shift currents[10–12] or the injection of free electrical currents.[13] Optical rectification is related to the nonresonant excitation of a polarization density and does not lead to the flow of a free charge current. Shift currents can be interpreted as arising from a photoinduced charge displacement. Free carrier current injection is related to the interference of absorption pathways associated with different optical polarizations and occurs in low symmetry materials such as wurtzite.

Optical rectification, shift, and injection currents also exist in the third-order nonlinear optical response of these materials.[10] Much attention has been paid to exploit these nonlinearities with harmonically related near-infrared fundamental and second harmonic pulses associated with parts of the nondegenerate third-order susceptibility $\chi^{(3)}(0;\omega,\omega,-2\omega)$ [in contrast, the degenerate susceptibility $\chi^{(3)}(\omega;\omega,-\omega,-\omega)$ is, e.g., related to the Kerr nonlinearity of the medium[14]]. While not much is known about third-order shift currents, third-order optical rectification has found application to generate Bragg gratings in optical fibers.[15] More strikingly, efficient current injection in GaAs has been predicted and observed illuminating GaAs (band-gap energy of 1.42 eV) with phase-related 0.8 eV/1.6 eV femtosecond pulse pairs.[6] This current injection process has been shown to be the resonant counterpart to third-order nonlinear rectification[16] and is associated with a motion of free charges over distances of about 10 nm, limited by the momentum relaxation time of charge carriers. In a microscopic picture, current injection can be understood as arising from quantum interference of one- and two-photon absorption pathways across the direct band gap.[17–19] The time derivative of the macroscopic injected current density induced by a harmonically related two-color light field is[17]

$$\dot{J}_i = 2\,\eta_{ijkl}E_j^{\omega}E_k^{\omega}E_l^{2\omega}\sin(2\Phi_{\omega}-\Phi_{2\omega}), \qquad (1)$$

where $E_{j,k}^{\omega}$ and $E_l^{2\omega}$ are the electric field amplitudes with Cartesian indices, i, j, k, and l, Φ_{ω} and $\Phi_{2\omega}$ are their phases, and η_{ijkl} is the total current injection tensor related to a divergent, imaginary part of $\chi^{(3)}(0;\omega,\omega,-2\omega)$. In a typical experimental configuration, currents are injected with pulses of $\sim$100 fs duration. The corresponding ultrafast currents act as an electromagnetic source term for far-infrared (terahertz) radiation. In a far-field electro-optic sampling experiment, the recorded terahertz field is proportional to the time derivative of the current in the specimen. The recorded terahertz trace is, therefore, a direct fingerprint of the charge motion in the sample.

In centrosymmetric media, the second-order optical nonlinearity is zero due to symmetry considerations. In contrast, all the third-order optical nonlinearities mentioned above are symmetry allowed. As an example, coherent control of terahertz radiation has been demonstrated even in ambient air.[20] In the present study, we analyze third-order photoinduced current in germanium and silicon. Germanium has a direct band gap of 0.8 eV and, therefore, effectively behaves as a direct semiconductor for the photon energies used here. However, the optical transitions generate carriers high in the conduction and valence bands, i.e., electrons and holes that experience ultrafast momentum relaxation. In silicon, for our photon energies, both single- and two-photon absorptions require phonon participation. As a result, the resonant optical transitions across the indirect band gap might also be of comparable strength to nonresonant sources (e.g., rectification) involving virtual excitations across the direct band gap. Recent results[7] indicate that current injection across the indirect band gap still dominates over the nonresonant third-order optical rectification, but detailed theoretical work is required to elucidate this relation.

III. EXPERIMENTAL SCHEME

The optical source for the all-optical current injection experiment is a 250 kHz Ti:sapphire regenerative amplifier combined with an optical parametric amplifier which produces 150 fs pulses with an average power of 50 mW and a tuning range between 1420 and 1800 nm (ω). A beta barium borate (BBO) crystal generates several milliwatts of second harmonic light (2ω).

It is important to relate these photon energies of 0.7 eV $\leqslant \hbar\omega \leqslant$ 0.9 eV to the room temperature band structure parameters of the semiconductors of the present study.[21] For the case of silicon, the photon energy of the fundamental beam is well below both the indirect ($E_{G,i}^{\mathrm{Si}}$=1.1 eV) and the direct ($E_{G,d}^{\mathrm{Si}}\approx$3.5 eV) gaps, whereas the second harmonic beam generates electron-hole pairs via phonon-assisted indirect transitions yielding electrons in the six degenerate conduction band minima near the X point. In contrast, the energy of the 2ω radiation is well above both the indirect ($E_{G,i}^{\mathrm{Ge}}$=0.66 eV) and the direct ($E_{G,d}^{\mathrm{Ge}}\approx$0.8 eV) band gaps of germanium, whereas the fundamental beam can be tuned across the direct gap.

As sketched in Fig. 1, the ω and 2ω pulse trains are spatially and temporally superimposed in a two-color Michelson interferometer. A piezoelectric transducer precisely controls the relative phase parameter $\Delta\Phi=2\Phi_{\omega}-\Phi_{2\omega}$. Polarization optics in the two arms of the interferometer allows for the adjustment of arbitrary polarization geometries of the two-color light field. The beams are focused to a 100 μm spot on the semiconductor layers at room temperature. In order to analyze the terahertz emission of the specimen, its radiation is collected with an off-axis parabolic mirror. Subsequently, the terahertz radiation is refocused into a 500 μm thick ZnTe crystal for electro-optic sampling.[22] The 150 fs probe beam with a wavelength of 800 nm is directly derived from the 250 kHz regenerative Ti:sapphire amplifier. The choice of this low noise probe pulse yields a sensitivity of the balanced detection system as high as $\Delta I/I = 1\times10^{-7}$ Hz$^{-1/2}$ independent of the operation wavelength of the optical parametric amplifier. In this setup, the real-time terahertz emission may be characterized with a spectral bandwidth of about 4 THz only limited by the small phase walkoff between the tera-

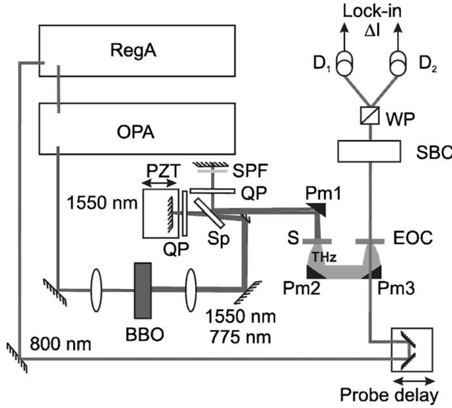

FIG. 1. Experimental setup for ultrafast current generation and detection. RegA: regenerative amplifier; OPA: optical parametric amplifier; BBO: beta barium borate frequency doubler; Sp: dichroic beam separator; QP: quarter wave plate; SPF: 1350 nm short pass filter; Pm: off-axis parabolic mirrors; S: semiconductor sample; EOC: ZnTe electro-optic crystal; SBC: Soleil-Babinet compensator; WP: Wollaston prism; D: photodiodes.

hertz transient and the near-infrared probe light in the ZnTe crystal.

IV. ALL-OPTICAL CURRENT INJECTION IN GERMANIUM

In this section, we demonstrate coherent control of directional electric currents in a 500 μm thick [100] oriented germanium wafer. The optical parametric amplifier is initially tuned to 1550 nm with a corresponding second harmonic wavelength of 775 nm. Taking into account one- and two-photon absorption coefficients of $\alpha^{\mathrm{Ge}}_{775\ \mathrm{nm}}=5.6\times10^{4}\ \mathrm{cm}^{-1}$ (Ref. 23) and $\beta^{\mathrm{Ge}}_{1550\ \mathrm{nm}}\approx100\ \mathrm{cm/GW}$,[24] carrier densities of $N^{2\omega}=1.1\times10^{18}\ \mathrm{cm}^{-3}$ and $N^{\omega}=5\times10^{18}\ \mathrm{cm}^{-3}$ are generated. As a result of these similar carrier densities generated via one- and two-photon absorptions, we expect a pronounced interference between these absorption pathways and, thus, a strong current injection.[25] Typical traces for the electro-optic signal (which is proportional to the terahertz field strength) of ultrafast currents generated by copolarized pulses at 1550/775 nm are displayed in Fig. 2(a). We observe a well resolved ultrafast burst of electromagnetic radiation with a phase that can be shifted by π depending on the relative phase adjustments of $\Delta\Phi=+\pi/2$ (black line) and $\Delta\Phi=-\pi/2$ (gray line) of the two-color pump field. We emphasize that this finding indicates a full inversion of the vector direction of the current flow induced solely by a change of the relative phase $\Delta\Phi$. The Fourier spectrum of the transient is displayed in Fig. 2(c) and reveals a broad emission around 2 THz which is cut off at around 3.5 THz due to the limited bandwidth of the electro-optic detection scheme (which is predominantly determined by the 500 μm thick electro-optic crystal used for terahertz detection). We note that the real source terms likely contain frequency components up to ~6 THz given by the bandwidth of the excitation pulse. The cutoff of the high-frequency part of the emission results in oscillations of the terahertz transients for later delay times [compare Fig. 2(a)], which are not directly related to the current dynamics in the sample. The actual time-resolved currents, as revealed by thinner electro-optic detection crystals (but yielding lower signal to noise), relax in <1 ps, reflecting ultrafast momentum relaxation of carriers. The switching time of this current is only limited by the pulse duration of the two-color excitation pulse, i.e., in the order of 150 fs in the present experiment. Moreover, the current is confined to the near surface region of 200 nm thickness determined by the strong absorption of the second harmonic light.

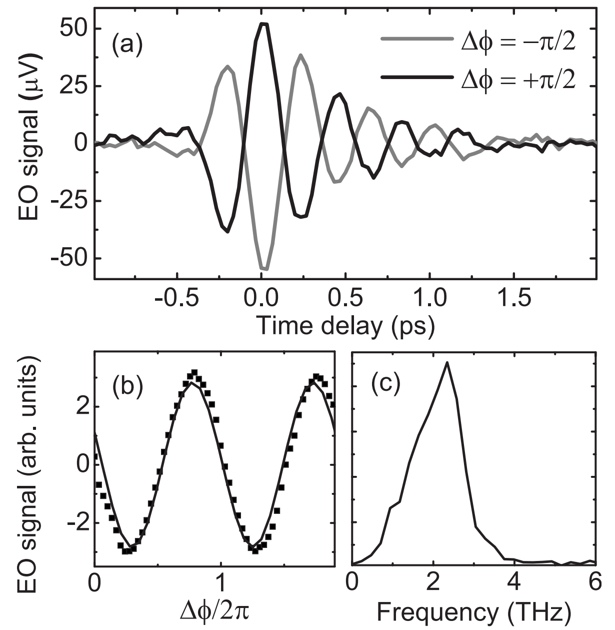

FIG. 2. Electro-optic signal (proportional to the terahertz field strength) from current injection in Ge. (a) Temporal trace of the detected terahertz field for two different values of the relative phase $\Delta\phi$. The carrier densities injected by the ω and 2ω pulses are $N^{\omega}=5\times10^{18}\ \mathrm{cm}^{-3}$ and $N^{2\omega}=1.1\times10^{18}\ \mathrm{cm}^{-3}$, respectively, and the fundamental wavelength is 1550 nm. (b) Field strength $E_{THz}(\Delta\Phi)$ at a fixed probe delay (squares) with a sinusoidal fit (solid line). (c) Fourier transform of the time-domain signal.

The dependence of the terahertz field amplitude as a function of the relative phase $\Delta\Phi=2\Phi_{\omega}-\Phi_{2\omega}$ of the two-color laser field is displayed in Fig. 2(b) and nicely follows a sinusoidal fit. This behavior is similar to the terahertz emission related to the quantum interference control of photocurrents in direct-gap materials such as GaAs.[6,17] However, in these direct band-gap materials, coherent control of directional currents has only been demonstrated utilizing electron and hole states near the band edges. In contrast, both the two-photon absorption of ω light and the one-photon absorption of 2ω light couple carriers high up in the band structure of germanium in the present case. Compared to the emission strength of a 1 μm GaAs layer (for this thickness, the major part of the 2ω radiation is absorbed), we find a signal reduction by a factor of ~15. This finding might be attributed to the larger effective masses of charge carriers in germanium as well as the stronger carrier-phonon scattering in the mul-

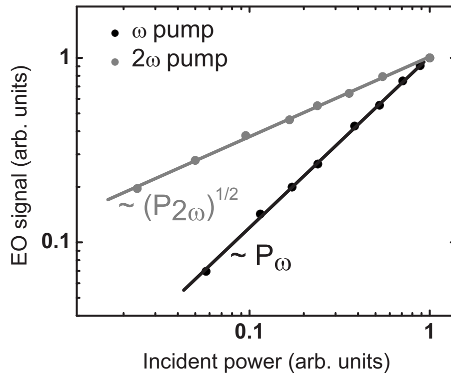

FIG. 3. Peak terahertz field strengths (dots) observed in germanium for various excitation powers of the fundamental and the second harmonic pulses. The solid lines correspond to the two different power scalings indicated in the graph.

tivalley conduction band with its Γ valley and the four degenerate L valleys. As a result, both the velocity of the photogenerated carriers and their scattering time are reduced in comparison with near-band edge excitation in a direct-gap semiconductor.

In order to verify the above $\chi^{(3)}$ behavior of an injection current-type interaction, we analyze the terahertz field amplitude for various excitation intensities. Figure 3 displays the normalized terahertz field amplitude for an independent variation of the incident intensity of the ω and the 2ω beams. Both curves nicely follow a power law with exponents near to 1.0 and 0.5 for the variation of the fundamental and the second harmonic intensities, respectively. Since the electro-optic sampling method is sensitive to the field variable E, this dependence is consistent with the third-order optical nonlinearity discussed in Eq. (1).

It is interesting to note that terahertz radiation is also observed by illuminating the sample with the fundamental beam alone (see Fig. 4 for the case of excitation with 1550 nm pulses). In contrast, terahertz emission related to an excitation with the rather weak 2ω beam alone is very small and close to the resolution limit of the experiment. As displayed in the inset of Fig. 4, a linear variation of the terahertz field with incident pump powers points to a $\chi^{(2)}$ type interaction with a saturation of the terahertz emission at high intensities. This result is surprising since $\chi^{(2)}$ is expected to vanish in germanium as a centrosymmetric material, although it could arise from surface-related effects. An in-plane rotation of the sample reveals a slight variation of the emission strength depending on the orientation of the light polarization with respect to the crystal axis. The terahertz emission is likely related to a moderate surface field E_{dc} which is well known to result in light-induced ultrafast charge displacements, e.g., in GaAs.[27] Such a static electric field along the propagation axis could yield a current density $J_i \propto \chi^{(3)}\ (0;\omega,-\omega,0)(E_x^{\omega})^2 E_{dc}$ and a corresponding ultrafast terahertz emission.[28] The interpretation as a surface-related phenomenon is supported by a clear influence of chemical surface etching (e.g., with HF) on this one-color-mediated process. We also note that similar experimental results have been reported recently:[29] this more detailed analysis of one-

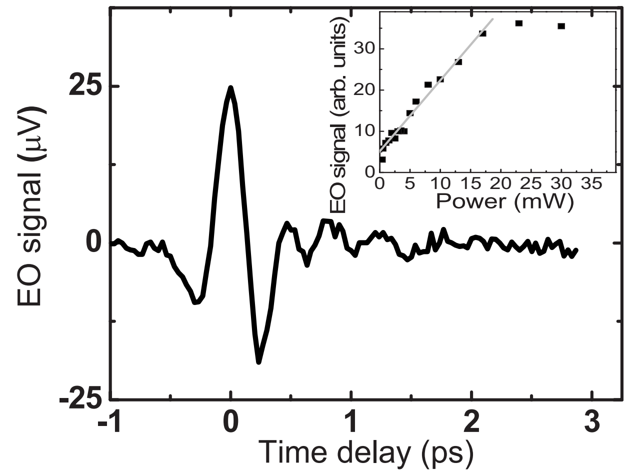

FIG. 4. Temporal trace of the detected terahertz field from the single-beam surface effect in Ge induced by the fundamental radiation of a wavelength of 1550 nm. The inset shows the emission strength for various average excitation powers with the solid line indicating a linear trend.

color-induced terahertz emission in germanium points to contributions of both the photo-Dember effect and surface fields.

We now turn to the wavelength dependence of the current injection in germanium. To this end, the operational wavelength of the optical parametric amplifier is varied from 1420 to 1800 nm. To account for the variation in the pulse intensity as well as the efficiency of the second harmonic generation, the data are corrected according to the intensity dependence of Eq. (1), i.e., the observed terahertz field strengths are divided by $P_{\omega}P_{2\omega}^{0.5}$ with P_{ω} and $P_{2\omega}$ being the average power of the fundamental and second harmonic radiation. This efficiency just serves to compare different materials and different excitation wavelengths and is not an absolute measure. As displayed in Fig. 5, quantum interference control of ballistic currents is possible throughout the entire spectral window of this study which also covers the important telecommunications window. The efficiency exhibits a

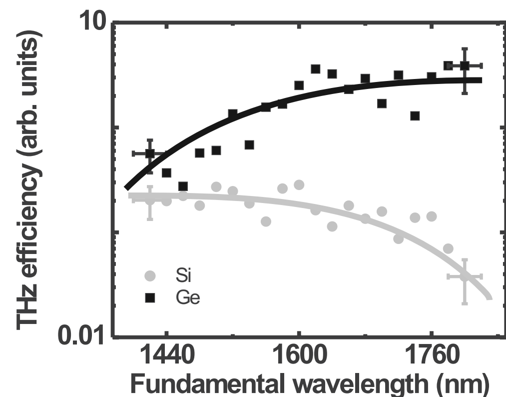

FIG. 5. Efficiency of the terahertz generation in a 125 μm thick silicon wafer and a 500 μm thick germanium wafer for various fundamental wavelengths (see definition of the efficiency in the main text). The solid curves are a guide to the eyes.

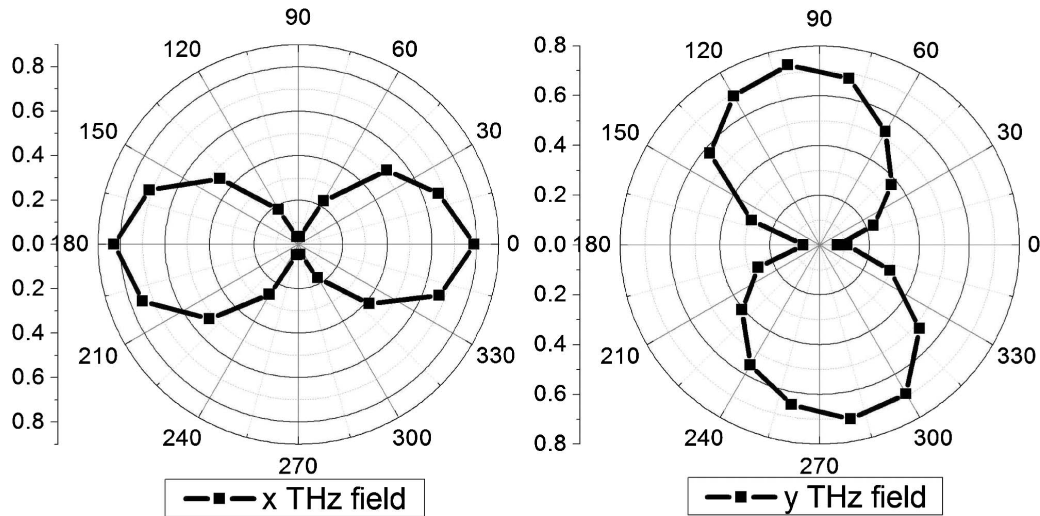

FIG. 6. Contour plots of the terahertz emission strength for various relative angles φ between the polarizations of the 1550 and 775 nm excitation field. (a) Strength of the horizontal (x) component of the terahertz field. (b) Corresponding vertical (y) component. The polarization of the second harmonic beam is kept at $\varphi=0°$, whereas the polarization of the fundamental beam is given by the angle φ indicated in the graph.

broad plateau for wavelengths between 1600 and 1800 nm, whereas the terahertz emission decreases significantly at shorter wavelengths. This finding is likely related to the competing process of direct one-photon absorption of the fundamental beam for these wavelengths which effectively reduces the number of photons available for the $\chi^{(3)}$ current injection process (note that the wavelength corresponding to the direct band gap of germanium is ~1550 nm). Although the carrier velocity and, thus, the current density increase with the photon energy, this trend might be partially compensated by the decrease of the momentum relaxation time with increasing excess energy. For a much longer wavelength corresponding to photons approaching half the band-gap energy, we expect a drastic reduction of the injection efficiency due to the small number of available final states. This regime, however, is not accessible with the limited tuning range of the optical parametric amplifier. We would like to note that additional experiments analyzing the terahertz emission in a reflection geometry point toward an emission strength of germanium, which, relative to silicon, is approximately three times larger than presented in the data of Fig. 5. This finding is likely related to a small residual terahertz absorption in the Ge wafer of this study.

Additional insight into the microscopic details of the all-optical current injection is provided by analyzing the polarization geometry. In particular, the two terahertz polarization components are resolved using a wire grid polarizer. The polarizations of the two excitation beams are controlled independently with polarization optics in the two-color Michelson interferometer. The results for numerous configurations are displayed as polar diagrams in Fig. 6. The polarization of the second harmonic beam is kept horizontally, whereas the polarization of the fundamental beam is rotated by an angle of φ. As a result, both the ω and the 2ω light are polarized along the horizontal (x) axis for $\varphi=0°$ (note, however, that the x and y directions used here are defined in the laboratory frame and are not related to a specific orientation with respect to the crystal axis). In this case, the strong terahertz emission is also polarized in this direction reflecting the ultrafast current flow along the common light polarization direction. This finding is consistent with the expectation that the maximum current is injected when the pump beams are copolarized, as occurs for GaAs.[17] At $\varphi=90°$, the polarization of the ω pulse is along the vertical (y) axis. For this cross-polarized excitation, we observe a y-polarized terahertz emission which is slightly smaller than that for the case of parallel polarizations. Apparently, the direction of the injected current is primarily governed by the polarization of the fundamental beam. The details of these polarization properties likely also depend on the precise orientation of the sample with respect to the crystal axis which has not been analyzed in detail here.

V. CURRENT INJECTION IN SILICON

We now turn to the all-optical generation of ballistic currents in silicon, wherein phonon participation is required to provide the momentum mismatch between the valence band maximum at the Γ point and the conduction band minima near the X point of the Brillouin zone.

Some of the observations have already been presented recently[7] and will only be summarized briefly here. The traces of the terahertz emission of thin silicon layers as well as its $\chi^{(3)}$-type power and phase dependence are qualitatively very similar to the properties of germanium presented in Figs. 2 and 3. Also, the analysis of the polarization configuration of the current injection in silicon reveals identical trends, as the findings in germanium shown in Fig. 6. Apparently, an efficient generation of directional currents is still possible via a quantum interference of one- and two-photon absorption pathways across the indirect band gap. Figure 5 compares the efficiency of the current injection in silicon and

germanium for various fundamental wavelengths. As a general trend, the terahertz emission of silicon is weaker than in germanium but not drastically reduced despite the distinctly different excitation mechanism. As the wavelength changes from 1420 to 1800 nm, the injection efficiency slowly decreases by a factor of ~3, i.e., the dispersion has the opposite trend as compared to germanium (see Fig. 5). This is likely related to the decreasing velocity of carriers photogenerated in silicon when $2\hbar\omega$ approaches the indirect band gap corresponding to a fundamental wavelength of 2.2 μm.

Silicon as an indirect semiconductor interacts weakly with light. Specifically, the linear absorption coefficient for a wavelength of 775 nm is $\sim 1300\ \mathrm{cm}^{-1}$ (Ref. 23) corresponding to a penetration depth of almost 10 μm. Similarly, at 1550 nm, the two-photon absorption coefficient of 0.75 cm/GW (Ref. 26) is more than 1 order of magnitude smaller than in GaAs. The all-optical current injection is, therefore, substantially affected by the phase mismatch within the two-color excitation field. In general, a difference in the phase velocities implies a phase walkoff of the two-color light field of

$$\Delta\Phi(z) = \Delta\Phi_0 + \frac{4\pi}{\lambda_\omega}(n_{2\omega} - n_\omega)z, \qquad (2)$$

where $\Delta\Phi_0$ is the relative phase at the semiconductor surface and z is the depth along the beam propagation axis. As an example, the refractive index for 1550 nm is $n^{\mathrm{Si}}_{1550\ \mathrm{nm}}=3.48$, whereas $n^{\mathrm{Si}}_{775\ \mathrm{nm}}=3.71$.[23] As a result, the coherence length is as small as ~2 μm. Therefore, the current flow in the semiconductor layer experiences a periodic reversal of the vector direction of the photoinjected current density as a function of z,

$$\dot{J}(z) \propto I_\omega(z)[I_{2\omega}(z)]^{1/2}\sin[\Delta\Phi(z)], \qquad (3)$$

where the depletion of the pump beams' intensity is described by $I_{2\omega}(z)=I_{2\omega}(0)e^{-\alpha_{2\omega}z}$ and $I_\omega(z)=\frac{I_\omega(0)}{1+\beta_\omega z I_\omega(0)} \approx I_\omega(0)e^{-\beta_\omega z I_\omega(0)}$. Since the detection of ultrafast currents is based on the emission of long wavelength electromagnetic radiation, a destructive interference of the terahertz emission of currents with different vector orientations is expected. Figure 7(a) depicts a simulation for the maximum total current flow in silicon and germanium for different layer thicknesses. These results are obtained by integrating the current density of Eq. (3) over the layer and maximizing the expression with respect to the external phase parameter $\Delta\Phi_0$. The maximum total current in silicon is observed for a film thickness ~2 μm, although only 10% of the incident light is absorbed within this depth. To verify this aspect experimentally, we have analyzed the current injection for silicon samples with different thicknesses. Specifically, we compare results from silicon-on-sapphire samples with thicknesses of 500 nm and 2 μm to results for a 125 μm thick wafer; all samples have [100] orientation. The observed maximum terahertz field amplitudes for the different silicon specimens are also displayed in Fig. 7(a) and are in good agreement with the simulated trend. Figure 7(b) shows a corresponding simulation for germanium and compares the actual dispersion of the refractive index with the case assuming ideal phase matching. In this material, phase matching only has a minor influence on the current injection since the penetration depth of the 2ω light is as small as 200 nm, i.e., much shorter than the phase-coherence length of the two-color excitation field.

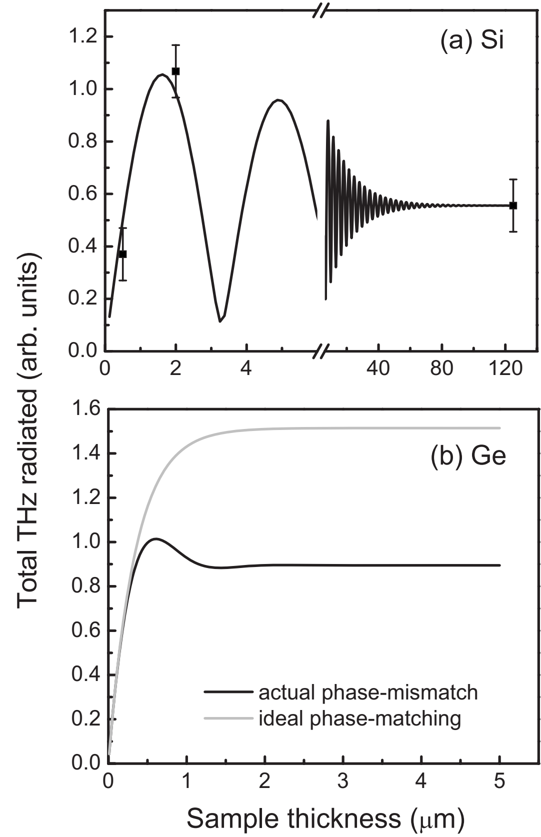

FIG. 7. Simulated terahertz field strength for different film thicknesses: (a) silicon and (b) germanium. Note the different scale of the abscissas. The squares in (a) indicate the relative emission strength observed for the three different silicon samples of the present study.

We have also studied the influence of the in-plane orientation θ on the efficiency of the current injection in a 125 μm thick [100] oriented silicon wafer. As depicted in Fig. 8, the amplitude of the terahertz emission does not change with the angle θ within the experimental accuracy. Apparently, the vector direction is almost exclusively determined by the polarization properties of the excitation field, whereas the orientation with respect to the crystal axis is of only minor importance. The dependence of the current injection on external optical parameters only should, therefore, in principle facilitate all-optical current generation in polycrystalline material.

VI. MICROSCOPIC PICTURE OF CURRENT INJECTION IN INDIRECT SEMICONDUCTORS

In a microscopic view, the all-optical injection of ballistic currents in direct-gap materials is well understood as arising

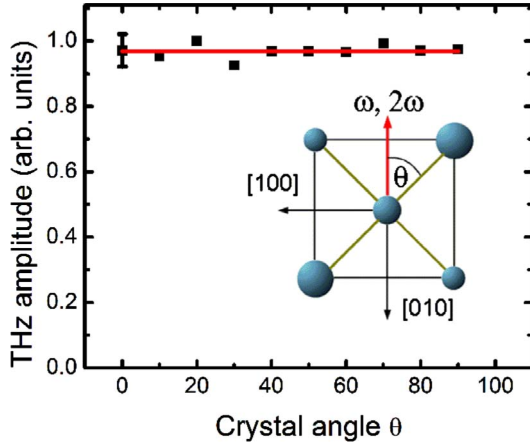

FIG. 8. (Color online) Terahertz field amplitude as a function of the in-plane orientation angle θ of the silicon layer. The inset shows a schematic of the crystal orientation and the polarization of the excitation field. Both the ω and the 2ω fields are polarized along the y axis and the y component of the terahertz radiation is detected. The error bar represents random errors as well as slight sample inhomogeneities. The size of the schematic ion cores reflects the position along the [001] axis.

from the quantum interference of one- and two-photon absorption processes. In this section, we will extend this picture to phonon-assisted transitions to provide a qualitative understanding of the response of indirect semiconductors to the excitation with harmonically related ultrashort laser pulses. We note that this section serves as a tentative explanation for the current injection in silicon. In the case of germanium, current injection is expected to occur predominantly via the much stronger direct optical transitions.

In a direct semiconductor, above band-gap photons directly couple valence and conduction band states via electrical dipole transitions. In the present experimental situation with a sub-band-gap fundamental pulse, only 2ω radiation induces one-photon transitions with an amplitude $a^{2\omega}(\mathbf{k}) \propto \langle v_{\mathbf{k}}|p|c_{\mathbf{k}}\rangle$ determined by the strength of the dipole matrix element between the valence band state $|v_{\mathbf{k}}\rangle$ and the conduction band state $|c_{\mathbf{k}}\rangle$. Note that this transition amplitude is even in $\mathbf{k}$ space, i.e., $a^{2\omega}(\mathbf{k})=a^{2\omega}(-\mathbf{k})$. In contrast, the properties of the two-photon absorption of ω are strongly affected by the need for an intermediate state in second-order perturbation theory. Neglecting higher electronic bands, only the initial valence band state $|v_{\mathbf{k}}\rangle$ or the final conduction band state $|c_{\mathbf{k}}\rangle$ can serve as such an intermediate state. Summing these two possibilities gives rise to a two-photon transition amplitude of

$$a^{\omega}(\mathbf{k}) \propto \langle v_{\mathbf{k}}|p|v_{\mathbf{k}}\rangle\langle v_{\mathbf{k}}|p|c_{\mathbf{k}}\rangle + \langle v_{\mathbf{k}}|p|c_{\mathbf{k}}\rangle\langle c_{\mathbf{k}}|p|c_{\mathbf{k}}\rangle. \quad (4)$$

Both the expressions $\langle v_{\mathbf{k}}|p|v_{\mathbf{k}}\rangle$ and $\langle c_{\mathbf{k}}|p|c_{\mathbf{k}}\rangle$ are proportional to the group velocity at this point of the band structure. As a result, these quantities change sign if $+\mathbf{k}$ changes to $-\mathbf{k}$. As a result, the two-photon induced transition rate is an odd function in $\mathbf{k}$, i.e., $a^{\omega}(-\mathbf{k})=-a^{\omega}(\mathbf{k})$. Summing up the one- and two-photon mediated absorption pathways gives rise to a carrier generation rate for a given position $\mathbf{k}$ in momentum space,

$$\dot{N}(\mathbf{k}) \propto |a^{2\omega}(\mathbf{k}) + a^{\omega}(\mathbf{k})|^2 = |a^{2\omega}(\mathbf{k})|^2 + |a^{\omega}(\mathbf{k})|^2 + 2\Re a^{2\omega}(\mathbf{k})[a^{\omega}(\mathbf{k})]^*. \quad (5)$$

If one sums $\dot{N}(\mathbf{k})$ over the Brillouin zone, the interference term results in the generation of a polar distribution in $\mathbf{k}$ space, i.e., the injection of a current. The total current density associated with the electron (e) or hole (h) current can be calculated by integrating Eq. (5) in momentum space,

$$\dot{J}_{e,h} = \sum_{\mathbf{k}} \dot{N}(\mathbf{k}) e v_{e,h}(\mathbf{k}). \quad (6)$$

The origin of a macroscopic current may be understood as both the group velocity $v_{e,h}(\mathbf{k})$ and the interference term $2\Re a^{2\omega}(a^{\omega})^*$ are odd functions in reciprocal space. It is interesting to note that the total number of photogenerated carriers is the sum of independent one- and two-photon absorption pathways, whereas the interference term only produces a redistribution in $\mathbf{k}$ space.

In an indirect semiconductor of high crystal quality, absorption is mainly facilitated using phonons to overcome the $\mathbf{k}$-space mismatch between the valence band maximum and the conduction band minimum. The theoretical description of one- and two-photon absorption pathways, therefore, relies on second- and third-order perturbation theories, respectively. We do not attempt to calculate all these processes in detail. Rather, we demonstrate that similar to the above discussion, the one- and two-photon transition amplitudes exhibit a transformation behavior in $\mathbf{k}$ space that allows for the quantum interference control of currents.

We now identify and analyze the dominant absorption channels for the case of an indirect semiconductor such as silicon. It is generally assumed that phonon-mediated interband transitions can be neglected, i.e., the transition from the valence to the conduction band is an optical one. Moreover, we only consider one valence and conduction band since transitions involving higher bands should be clearly weaker due to the large energy mismatch of the intermediate states (which implies unfavorable energy denominators in the transition amplitudes, as calculated in perturbation theory). The remaining processes are summarized in Fig. 9. As shown in Fig. 9(a), linear absorption in an indirect semiconductor couples, e.g., a valence band state $|v_{\mathbf{k}}\rangle$ to a conduction band state $|c_{\mathbf{k+q}}\rangle$ with $\mathbf{q}$ being the momentum of the phonon emitted or absorbed in the transition. In second-order perturbation theory, the transition amplitude for this process is $a_j^{2\omega}(\mathbf{k},\mathbf{q}) \propto \langle v_{\mathbf{k}}|p|c_{\mathbf{k}}\rangle\langle c_{\mathbf{k}}|H_{ep,j}|c_{\mathbf{k+q}}\rangle$ with an electron-phonon coupling $H_{ep,j}$ for a particular phonon branch j. The matrix element for carrier-phonon interaction depends only on the absolute value $|\mathbf{q}|$ of the momentum exchange.[30] Therefore, the transition amplitude satisfies

$$a_j^{2\omega}(-\mathbf{k},|\mathbf{q}|) = a_j^{2\omega}(\mathbf{k},|\mathbf{q}|). \quad (7)$$

For the case of two-photon transitions between the same states $|v_{\mathbf{k}}\rangle$ and $|c_{\mathbf{k+q}}\rangle$, i.e., an absorption mediated by ω radiation, the situation is complicated by the additional inter-

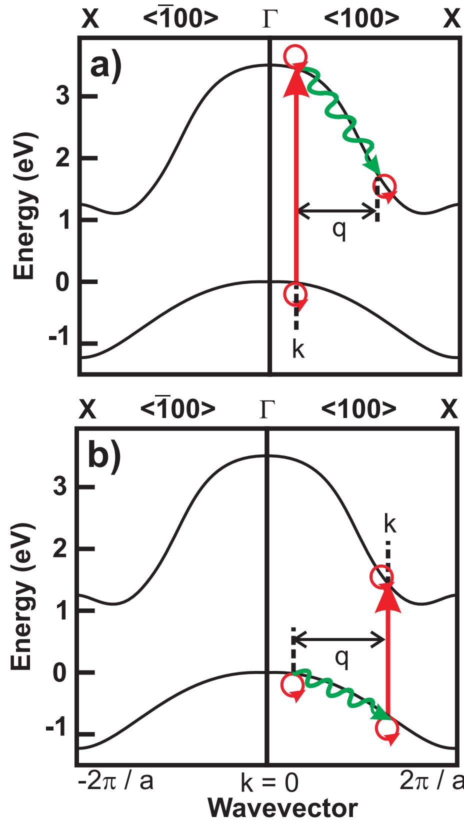

FIG. 9. (Color online) Schematic illustrations of the band structure of silicon with the relevant interband transitions. Vertical arrows indicate optical transitions induced by either ω or 2ω radiation. Closed loops correspond to optical self-scattering relevant for two-photon absorption pathways. Please note that each two-photon absorption pathways relies on one self-scattering process only. The wiggled lines represent phonon absorption or emission processes.

mediate state either in the conduction or valence band. However, for a process as depicted in Fig. 9(a), there are only three candidates for this intermediate state, namely, the initial state $|v_{\mathbf{k}}\rangle$, the intermediate state $|c_{\mathbf{k}}\rangle$, or the final state $|c_{\mathbf{k+q}}\rangle$. Summing up these three pathways in third-order perturbation theory yields a two-photon induced transition amplitude of

$$a_j^{\omega}(\mathbf{k},\mathbf{q}) \propto \langle v_{\mathbf{k}}|p|v_{\mathbf{k}}\rangle\langle v_{\mathbf{k}}|p|c_{\mathbf{k}}\rangle\langle c_{\mathbf{k}}|H_{ep,j}|c_{\mathbf{k+q}}\rangle + \langle v_{\mathbf{k}}|p|c_{\mathbf{k}}\rangle\langle c_{\mathbf{k}}|p|c_{\mathbf{k}}\rangle\langle c_{\mathbf{k}}|H_{ep,j}|c_{\mathbf{k+q}}\rangle + \langle v_{\mathbf{k}}|p|c_{\mathbf{k}}\rangle\langle c_{\mathbf{k}}|H_{ep,j}|c_{\mathbf{k+q}}\rangle\langle c_{\mathbf{k+q}}|p|c_{\mathbf{k+q}}\rangle. \quad (8)$$

Note that these contributions contain factors $\langle v_{\mathbf{k}}|p|v_{\mathbf{k}}\rangle$, $\langle c_{\mathbf{k}}|p|c_{\mathbf{k}}\rangle$, and $\langle c_{\mathbf{k+q}}|p|c_{\mathbf{k+q}}\rangle$, which are proportional to the group velocity of carriers at this position in $\mathbf{k}$ space. As a result, these quantities reverse sign when $(\mathbf{k},|\mathbf{q}|)$ changes to $(-\mathbf{k},|\mathbf{q}|)$. More strikingly, also, the entire transition amplitude satisfies

$$a_j^{\omega}(-\mathbf{k},|\mathbf{q}|) = -a_j^{\omega}(\mathbf{k},|\mathbf{q}|). \quad (9)$$

It should be noted that indirect optical transitions also occur with an intermediate state near the X point of the valence band [compare the schematical transitions in Fig. 9(b)]. Labeling the $\mathbf{k}$-space position of the vertical optical transitions with $\mathbf{k}$ and the initial state in the valence band with $\mathbf{k+q}$, it is straightforward to see that the above derivation as well as the transformation behavior in reciprocal space is also valid for these types of processes.

In essence, this derivation shows that the property of the one- and two-photon absorption amplitudes in direct-gap transitions to be even and odd in $\mathbf{k}$ space, respectively, can be extended to the case of an indirect material. As a consequence, the total transition amplitude as calculated in Eq. (4) contains interference contributions which yield a polar distribution in reciprocal space also in the case of indirect optical transitions. Current injection is, therefore, possible in the same way as in a direct band-gap material. The interference contrast, however, is likely reduced, e.g., by the multitude of phonon branches j contributing to the optical absorption. Experimentally, it has been observed that the density of the photogenerated current in silicon is reduced by a factor of ~50 with respect to the model system GaAs.[7] Taking into account the approximately ten times smaller absorption of silicon and the relatively large effective masses and, correspondingly, large carrier scattering rates, the quantum efficiency of the current injection across the indirect band gap is remarkably high.

Finally, we would like to propose a more intuitive picture why current injection might occur across an indirect band gap. As visualized in Fig. 9, only either electrons or holes experience phonon scattering for any given type of optical transition considered here. Without special assumptions on the properties of the carrier-phonon interaction, the current contribution of this carrier type is expected to be very small since phonon scattering strongly reduces any directional preference. In contrast, the carrier type that is not subject to phonon scattering still contributes to the current since the transformation behavior of the transition amplitudes driving the interference phenomenon is also valid for indirect optical transitions. However, the theoretical details of this current injection across an indirect band gap need to be explicitly calculated.

VII. CONCLUSION

We have demonstrated all-optical control over the charge motion in the important group IV semiconductors silicon and germanium. Illuminating semiconductor layers with harmonically related near-infrared pulses yield the generation of a ballistic directional current flow on a subpicosecond time scale. The amplitude and the vector directions of the current are controlled by amplitude, polarization, and relative phase of the two-color excitation field. The theoretical description calls for an extension of the established injection current model for direct-gap semiconductors. A preliminary analysis in second- and third-order perturbation theories reveals the possibility to generate such polar carrier distributions across an indirect band gap. As a result, the current injection seems to be robust with respect to including phonons in the optical transitions.

The present technique represents the fastest way to generate charge currents, which can be located wherever one can

focus an optical beam and which are not governed by the location, inductance or capacitance effects of electrical contacts. It is possible that strain or quantum confinement might improve the efficiency of the current generation process or even allow more efficient current generation via a $\chi^{(2)}$ mediated single-beam technique. Finally, the results link near-infrared and terahertz technologies within the versatile silicon platform.

ACKNOWLEDGMENTS

We gratefully acknowledge valuable discussions with A. D. Bristow, J. E. Sipe, and A. L. Smirl. Financial support of the Natural Sciences and Engineering Research Council of Canada is gratefully appreciated. M.B. acknowledges support by the Alexander von Humboldt Foundation.

[1] L. Pavesi and D. J. Lockwood, *Silicon Photonics* (Springer, New York, 2004).

[2] H. Rong, R. Jones, A. Liu, O. Cohen, D. Hak, A. Fang, and M. Paniccia, Nature (London) **433**, 725 (2005).

[3] M. A. Foster, A. C. Turner, J. E. Sharping, B. S. Schmidt, M. Lipson, and A. L. Gaeta, Nature (London) **441**, 960 (2006).

[4] Q. Xu, B. Schmidt, S. Pradham, and M. Lipson, Nature (London) **435**, 235 (2005).

[5] R. S. Jacobsen, K. N. Andersen, P. I. Borel, J. Fage-Pedersen, L. H. Frandsen, O. Hansen, M. Kristensen, A. V. Lavrinenko, G. Moulin, H. Ou, C. Peucheret, B. Zsigri, and A. Bjarklev, Nature (London) **441**, 199 (2006).

[6] A. Haché, Y. Kostoulas, R. Atanasov, J. L. P. Hughes, J. E. Sipe, and H. M. van Driel, Phys. Rev. Lett. **78**, 306 (1997).

[7] L. Costa, M. Betz, M. Spasenović, A. D. Bristow, and H. M. van Driel, Nat. Phys. **3**, 632 (2007).

[8] A. Rice, Y. Jin, F. Ma, X.-C. Zhang, D. Bliss, J. Larkin, and M. Alexander, Appl. Phys. Lett. **64**, 1324 (1994).

[9] A. Nahata, A. S. Weling, and T. F. Heinz, Appl. Phys. Lett. **69**, 2321 (1996).

[10] C. Aversa and J. E. Sipe, IEEE J. Quantum Electron. **32**, 1570 (1996).

[11] J. E. Sipe and A. I. Shkrebtii, Phys. Rev. B **61**, 5337 (2000).

[12] D. Côté, N. Laman, and H. M. van Driel, Appl. Phys. Lett. **80**, 905 (2002).

[13] N. Laman, A. I. Shkrebtii, J. E. Sipe, and H. M. van Driel, Appl. Phys. Lett. **75**, 2581 (1999).

[14] D. J. Moss, J. E. Sipe, and H. M. van Driel, Phys. Rev. B **36**, 1153 (1987).

[15] R. H. Stolen and H. W. K. Tom, Opt. Lett. **12**, 585 (1987).

[16] M. Sheik-Bahae, Phys. Rev. B **60**, R11257 (1999).

[17] R. Atanasov, A. Haché, J. L. P. Hughes, H. M. van Driel, and J. E. Sipe, Phys. Rev. Lett. **76**, 1703 (1996).

[18] H. M. van Driel and J. E. Sipe, in *Ultrafast Phenomena in Semiconductors*, edited by K. T. Tsen (Springer, New York, 2001), p. 261.

[19] H. T. Duc, T. Meier, and S. W. Koch, Phys. Rev. Lett. **95**, 086606 (2005).

[20] X. Xie, J. Dai, and X.-C. Zhang, Phys. Rev. Lett. **96**, 075005 (2006).

[21] J. R. Chelikowsky and M. L. Cohen, Phys. Rev. B **14**, 556 (1976).

[22] Q. Wu and X.-C. Zhang, Appl. Phys. Lett. **67**, 3523 (1995).

[23] E. D. Palik, *Handbook of Optical Constants of Solids* (Academic, New York, 1985).

[24] R. Laenen, K. Simeonidis, and C. Rauscher, IEEE J. Sel. Top. Quantum Electron. **2**, 487 (1996).

[25] A. Haché, J. E. Sipe, and H. M. van Driel, IEEE J. Quantum Electron. **34**, 1144 (1998).

[26] A. D. Bristow, N. Rotenberg, and H. M. van Driel, Appl. Phys. Lett. **90**, 191104 (2007).

[27] T. Dekorsy, T. Pfeifer, W. Kütt, and H. Kurz, Phys. Rev. B **47**, 3842 (1993).

[28] S. L. Chuang, S. Schmitt-Rink, B. I. Greene, P. N. Saeta, and A. F. J. Levi, Phys. Rev. Lett. **68**, 102 (1992).

[29] A. Urbanovic, A. Krotkus, A. Adomavicius, and V. L. Malevich, Physica B **398**, 98 (2007).

[30] B. K. Ridley, *Quantum Processes in Semiconductors* (Clarendon, Oxford, 1988).